Construction and Building Materials 371 (2023) 130441

Contents lists available at ScienceDirect

Construction and Building Materials

journal homepage: www.elsevier.com/locate/conbuildmat

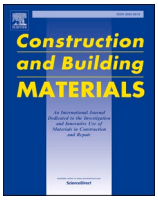

Lightweight ultra-high-performance concrete (UHPC) with expanded glass aggregate: Development, characterization, and life-cycle assessment

Pengwei Guo [a], Weina Meng [a,*], Jiang Du [a], Lily Stevenson [a], Baoguo Han [b], Yi Bao [a]

[a] Department of Civil, Environmental and Ocean Engineering, Stevens Institute of Technology, Hoboken, NJ 07030, United States
[b] School of Civil Engineering, Dalian University of Technology, Dalian, 116024, China

ARTICLE INFO

Keywords:
Ultra-high-performance concrete (UHPC)
Expanded glass
Glass microsphere
Internal curing
Lightweight
Polyethylene fiber

ABSTRACT

Ultra-high-performance concrete (UHPC) has high mechanical strengths and durability, but its density and carbon footprint are usually high. This paper developed a lightweight UHPC with low cost, low carbon footprint, low energy consumption, low thermal conductivity, and high ductility, by using three types of lightweight ingredients: hollow glass microsphere (460 kg/m^3), expanded glass aggregate (800 kg/m^3), and polyethylene fibers (970 kg/m^3). Underlying mechanisms were investigated through thermogravimetry, X-ray diffraction, and mercury intrusion porosimetry analyses. Results showed that the hollow glass microsphere reduced the thermal conductivity of concrete; the expanded glass aggregate mitigated shrinkage while enhancing compressive strengths and flexural properties of concrete through internal curing; and the polyethylene fibers promoted multiple cracks, increasing ductility and toughness of concrete. With 20 % hollow glass microsphere, 1.5 % polyethylene fiber, and 25 % expanded glass, UHPC mixtures were developed to achieve high compressive strength (>127 MPa) and high flexural strength (>21 MPa), while reducing the density by 20 % and carbon footprint by 16 % as well as embodied energy by 27 %.

1. Introduction

Ultra-high-performance concrete (UHPC) has high compressive strength (>120 MPa) [1] and high flexural strength (>15 MPa), as well as excellent durability due to the high particle packing density [2]. UHPC exhibits strain-hardening behavior by using chopped fibers [3]. Due to the dense microstructure, UHPC has high resistance to transport and attack of chemicals [4], but the density (2,500–2,650 kg/m^3) is 10 % higher than that of conventional concrete [5]. In North America, UHPC has been used in construction and rehabilitation of bridge girders and decks [2]. Reducing the density will increase the efficiency of transportation, lifting, and assembling of UHPC in construction, and reduce the self-weight of structures.

Typically, the lightweight ingredients are used in conventional concrete to reduce the density, as summarized in Table 1. To develop lightweight UHPC, one concern is that the use of lightweight ingredients compromises the mechanical strengths due to two mechanisms: (1) The pozzolanic reactivity of lightweight materials is low, such as glass microsphere It reduces the potential formation of hydration products such as calcium silicate hydrate [6]. (2) Lightweight ingredients are porous and fragile. For example, the crushing resistance of expanded glass aggregate is only 3 MPa [7]. It is difficult to reduce the density of UHPC while maintaining high mechanical properties.

The tradeoff of density and mechanical strengths imposes challenges in development of lightweight UHPC. Lu et al. used hollow glass microsphere to replace up to 50 % cement for lightweight UHPC [6]. Low water-to-binder ratio (<0.14) and sand-to-binder ratio (<0.2) were used to retain a high compressive strength (>120 MPa) due to the low reactivity of hollow glass microsphere [6]. However, high binder contents can highly increase shrinkage, water reducer demand, cost, and carbon footprint. Similarly, the use of lightweight aggregate compromises the strength of UHPC as well, while low water-to-binder ratio is needed to keep high mechanical properties [24]. Internal curing effect is a promising method to use lightweight aggregate for improving mechanical properties while reducing high shrinkage of UHPC. It was found that using pre-saturated lightweight sand to replace 25 % river sand increased the 28-d compressive strength by 18 % and reduced the autogenous shrinkage by 36 % [25]. However, the density of UHPC developed by pre-saturated lightweight shale aggregate presented in exiting studies are still as high as 2,300 kg/m^3 [24]. Expanded glass is an alternative material for conventional lightweight shale aggregate due to extremely low specific gravity. However, limited study is available on

* Corresponding author.
E-mail address: weina.meng@stevens.edu (W. Meng).

https://doi.org/10.1016/j.conbuildmat.2023.130441
Received 3 October 2022; Received in revised form 27 December 2022; Accepted 16 January 2023
Available online 28 February 2023

the effectiveness of expanded glass aggregate for the design of lightweight UHPC. It is not clear how the use of pre-saturated expanded glass as aggregate affects the internal curing effect, thus influencing the fresh and hardened properties of UHPC, because it has interconnected pores.

Ductility is considered because there is a correlation between ductility and durability [26]. The addition of polyethylene fibers is beneficial to improve the ductility of the concrete. Increasing ductility reduces crack widths and permeability of cracked matrix while promoting self-healing through secondary hydration [26]. Increasing ductility is aligned with improving sustainability because the maintenance cost will be reduced. Increasing ductility also benefits structural safety and resilience to hazards such as earthquake [27]. The brittleness of lightweight material increasing the potential of sudden failure of the concrete [28]. PE fiber is able to reduce the brittleness of the concrete [28]. In addition, due to low specific gravity, the PE fiber benefits the density of UHPC.

This research aims to develop UHPC mixtures with low density, low thermal conductivity, high mechanical strengths, high ductility, and high sustainability. The most important thing is to explore the maximum usage of expanded glass as internal curing in UHPC. This research adopted hollow glass microsphere, porous expanded glass aggregate, and PE fibers, whose specific gravity are 0.46, 0.80, and 0.97, respectively (Fig. 1). This research has multiple contributions: (1) Application of low-grained and low-density expanded glass aggregates to the design of lightweight UHPC. (2) Investigating the internal curing effect of expanded glass on the fresh and hardened properties of lightweight UHPC. (3) Investigating thermal conductivity of lightweight UHPC designed with different types of lightweight materials. (4) Performing comprehensive life cycle assessment to identify the benefits of the different lightweight ingredients on cost, energy conservation and carbon footprint.

To address this knowledge gap, this research investigates the effects of expanded glass aggregate on the autogenous shrinkage, mechanical properties, thermal properties, and durability of UHPC. The mechanisms are uncovered via measurements of internal relative humidity (IRH), isothermal calorimetry, thermogravimetric analysis (TGA), X-ray diffraction (XRD), and mercury intrusion porosimetry (MIP). Life cycle assessment was conducted to analyze the economic and environmental impacts.

2. Materials and mixture design

2.1. Materials

Type I Portland cement and slag from local plants were used as cementitious materials. Hollow glass microsphere (Im16K, 3M) made of soda-lime-borosilicate glass was adopted. The glass microsphere had a hollow spherical structure and thin wall. The expanded glass aggregate was porous and made of waste glass [29,30]. Both glass microsphere and expanded glass were prone to breakage during stirring [6]. A small part of the water may be released from pre-saturated expanded glass, and the usage of HRWR needs to be well controlled. The chemical composition and the physical properties of selected materials are listed in Table 2.

The specific gravity of the cement, slag, glass microsphere, expanded glass aggregate, and quartz sand were 3.15, 0.32, 2.90, 0.80, and 2.65, respectively. Two types of fibers, which are PE fibers and steel fibers, were adopted. The physical properties of the PE fibers and the steel fibers are shown in Table 3.

The particle size distributions of dry ingredients are shown in Fig. 2, The particle sizes of expanded glass and quartz sand were comparable. A polycarboxylate-based high-range water reducer (HRWR) with 34.4 % solid content was used to maintain high flowability (mortar with mini-slump spread of 280 mm). To be used as internal curing agent, the expanded glass was soaked in the water for 24 h to achieve a water-retention state [5]. The additional amount of water added is the total amount of water required to reach saturated-surface-dry (SSD) state of dry expanded glass minus the initial water content of expanded glass. The initial water content was measured according to ASTM C128 [31]. The pre-saturated expanded glass aggregate was sealed in a plastic bag for 24 h before use.

2.2. Mixture design

This research intends to reduce the self-weight of UHPC by synergistically reducing the weight of binder, aggregate, and fiber. Table 4 lists six mixtures designed with different types of lightweight ingredients. The control mixture is a developed sustainable UHPC mixture that used high-volume slag and full replacement of quartz sand by river sand [32]. Cement and slag respectively accounted for 40 % and 60 % of the binder volume in the control mixture. To reduce the weight of binder, 20 % slag was replaced by glass microsphere in mixture GM20. In mixtures L0 to L100, pre-saturated expanded glass was used as sand replacement from 0 to 100 %, and the steel fibers were fully replaced by the PE fibers. The sand-to-binder ratio was fixed at 0.6. The water absorption ratio of the expanded glass was 35 %. The internal curing water provided by expanded glass in mixtures L25, L50, and L100 was 19.6 g, 56.0 g, and 112.2 g, respectively.

2.3. Mixing, casting, and curing

A Hobart mortar mixer (capacity:12 L) was used to mix the mixtures in four steps: (1) mixing dry ingredients at 61 rpm for 3 min; (2) adding 90 % water and 90 % HRWR and mixing at 61 rpm for 3 min; (3) adding the remaining 10 % water and 10 % HRWR, and mixing at 113 rpm for 3 min; and (4) adding fibers at 61 rpm within 2 min and mixing for 1 min. The mixing was completed within 12 min. After casting, the molds were covered by plastic sheet and demolded after 24 h. After demolding, the samples were cured in saturated limewater at room temperature (23 ± 2 °C) until testing.

Table 1
Typical lightweight material used in concrete.

Materials	Size (μm)	Specific gravity	Replacement percentage	Composition	Strength decrease	References
Glass microsphere	18–65	0.125–0.6	0–100 %	Binder/ Aggregate	0–60 %	[6,8–10]
Fly ash cenosphere	120	0.4–0.8	0–100 %	Aggregate	0–17 %	[11,12]
Expanded perlite	0–4,750	1.1–1.4	0–100 %	Binder/ Aggregate	0–99 %	[13–15]
Expanded clay	0–4,750	0.96–1.8	0–100 %	Aggregate	0–77 %	[16,17]
Expanded glass	0–4,750	0.225–0.8	0–100 %	Aggregate	0–56 %	[18–20]
Foam glass	0–4,750	0.3–0.8	0–100 %	Aggregate	0–50 %	[21]
Expanded shale aggregate	0–4,750	1.07	0–100 %	Aggregate	0–59 %	[16]
Granulate fly ash aggregate	0–8,000	1.35	0–50 %	Aggregate	0–40 %	[22]
Natural pumice	0–20,000	0.6	0–100 %	Aggregate	0–75 %	[23]

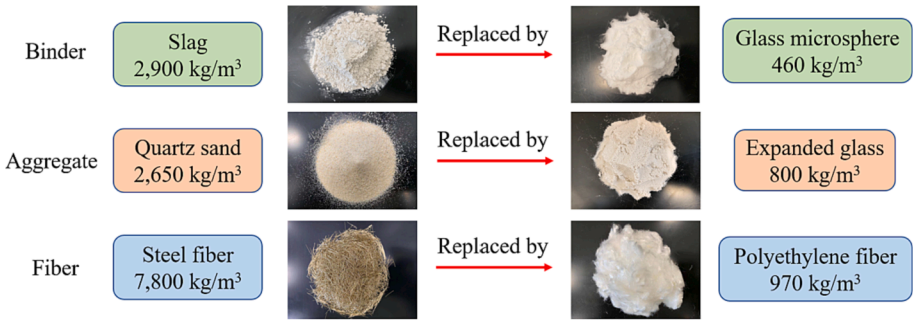

Fig. 1. Development of lightweight UHPC by the combined use of lightweight ingredients.

Table 2
Chemical of physical properties of cementitious materials and aggregate.

Composition	Cement	Glass microsphere	Slag	Expanded glass	Quartz sand
SiO_2 (%)	22.4	70–80	36.21	70–75	80.13
Al_2O_3 (%)	2.76	–	11.10	0.5–5	10.72
Fe_2O_3 (%)	2.24	–	0.76	–	2.89
CaO (%)	68.05	5–15	43.75	7–11	1.45
MgO (%)	0.91	–	5.09	0–5	2.01
SO_3 (%)	2.25	–	2.21	–	1.14
B_2O_3 (%)	0.30	2–6	0.63	–	–
Na_2O (eq)* (%)	0.14	3–8	0.58	10–19	–
Loss of ignition (%)	5.83	–	–	<0.5	–
Specific gravity	3.15	0.46	2.90	0.8	2.65
D_{50} (μm)	18	20	22	240	220

3. Experimental program

3.1. Pozzolanic reactivity

The Chapelle test was conducted to evaluate the pozzolanic reactivity of glass microsphere and expanded glass [33], in accordance with NF P18-513 [34]. In the test, 1 g test material and 1 g $Ca(OH)_2$ (CH in short) were added to 250 mL distilled water and boiled at 90 °C for 16 h. Meanwhile, stirring was continuously applied to promote pozzolanic reaction. The consumption of CH is used to quantify the pozzolanic reactivity, which is measured by titration of acid solutions.

3.2. Internal relative humidity and autogenous shrinkage

The internal relative humidity (IRH) was evaluated using prism specimens measuring 285 mm × 75 mm × 75 mm. For the preparation of the prism specimens, immediately after casting of the specimens, PVC tubes were inserted into the specimens at a depth of 40 mm to create holes [5]. A plastic film is used to cover the bottom of the PVC tube to

Table 3
Physical properties of steel and PE fibers.

	Length (mm)	Diameter (μm)	Density (kg/m³)	Elastic modulus (GPa)	Tensile strength (MPa)	Elongation (%)
Steel fiber	13	200	7,800	210	2,850	–
PE fiber	6	18	970	151	3,400	< 4.0 %

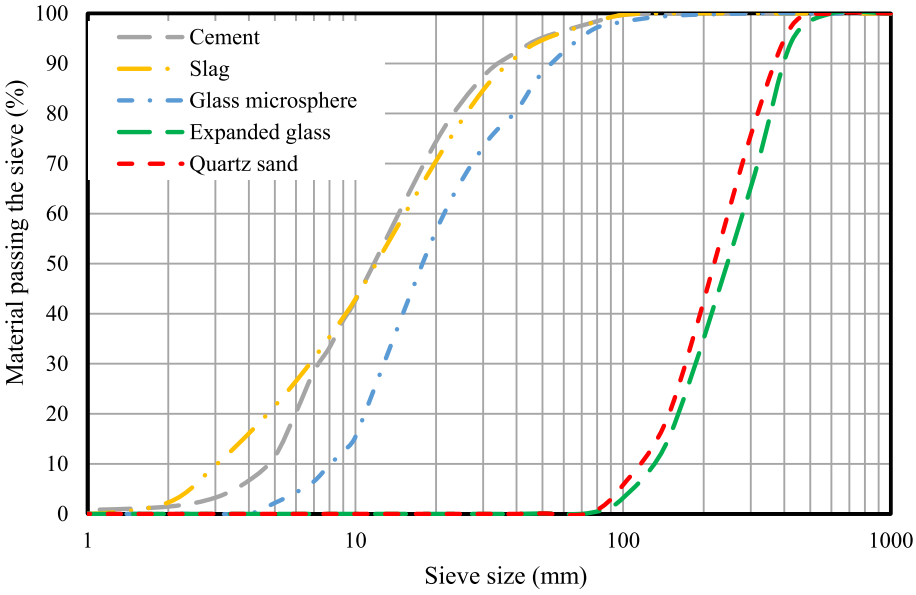

Fig. 2. Particle size distributions of dry ingredients used to prepare the UHPC mixtures.

Table 4
UHPC mixture design (kg/m^3).

Mixture	Cement	Slag	Glass microsphere	River sand	Expanded glass	HRWR	Water	PE fiber	Steel fiber
Control	565.1	780.4	0	780.4	0	40.5	225.1	0	117.0
GM20	565.1	520.3	41.3	780.4	0	34.0	227.9	0	117.0
L0	565.1	520.3	41.3	780.4	0	34.0	225.1	14.6	0
L25	565.1	520.3	41.3	557.1	56.1	28.4	232.6	14.6	0
L50	565.1	520.3	41.3	371.4	112.1	19.4	238.5	14.6	0
L100	565.1	520.3	41.3	0	224.3	11.5	243.6	14.6	0

prevent the intrusion of the fresh concrete. At initial setting, relative humidity sensors were placed into the holes to test the IRH at the middle depth of the specimens. A lid is applied to cover the top of the PVC tube to prevent the evaporation. Relative humidity meters take readings by touching the chip on the sensor. The relative humidity is tested with a time interval of 12 h. The testing setup is shown in Fig. 3.

The autogenous shrinkage of the mixtures was tested using sealed prism specimens in accordance with ASTM C1698 [35]. The samples were immediately sealed with foil and tape after they were demolded to prevent moisture loss. The shrinkage was recorded on a daily basis until 28 d.

3.3. Hydration heat

The heat of hydration of the investigated mixtures was evaluated using a calorimeter (Calmetrix HPC-4000) under the isothermal condition. For each mixture, about 60 g fresh sample was put into a plastic box and placed in the equipment for testing until 48 h.

3.4. Density and mechanical properties

The density of hardened UHPC mixtures was tested using cube specimens measuring 51 mm × 51 mm × 51 mm, according to BS EN 12390-7:2019 [36]. The density was calculated by dividing the mass by the volume of the cube specimens. The volume was measured using the water displacement method, and the mass was weighted using a high-precision balance.

The compressive strength of the mixtures at curing ages 1 d, 3 d, 7 d, 28 d, and 91 d was measured using cube specimens measuring 51 mm × 51 mm × 51 mm, according to ASTM C109 [37]. Prism specimens measuring 304.8 mm × 76.2 mm × 12.7 mm were used to test the 28-d flexural strengths, according to ASTM C1609 [38]. The equivalent flexural strength was calculated by Eq. (1).

$$\sigma = \frac{3F(L - L_i)}{2bd^2} \quad (1)$$

where b and d are the width and thickness of the beam; L is the supported span length; L_i is the length of loading span; F is the loading force at the fracture point; and σ is the flexural strength. In this research, $L = 240$ mm, $L_i = 94$ mm, $b = 76.2$ mm, and $d = 12.7$ mm.

3.5. Thermal conductivity

The thermal conductivity of the mixtures was tested using cube specimens measuring 51 mm × 51 mm × 51 mm, using the transient plane source method [39]. For each mixture, the test was repeated for 10 times, and the results were averaged.

3.6. Alkali-silica reactivity

Expansion of the mixtures due to the alkali-silica reaction was measured using mortar bars in accordance with ASTM C 1260 [40]. The mortar bars were cured for 24 h and then immersed in 1 M NaOH solution at 80 °C for 14 d. A length expansion <0.1 % was desired to avoid detrimental effects due to expansive deformations.

3.7. Microstructural characterization

At 28 d, cube specimens measuring 5 mm × 5 mm × 5 mm were collected from the hardened specimens and grounded into powder, to characterize the porosity and hydration products. The porosity was measured via MIP (Anton Paar). Porosity is determined based on the volume of mercury immersed in the voids of samples under pressure. The hydration products were evaluated via TGA (TGA 55). About 60 mg powder were heated to 1000 ℃ in nitrogen. The mass loss versus temperature data were recorded. Samples for MIP and TGA tests were immersed in 99.8 % isopropyl alcohol and dried at 50 ℃ for 24 h before testing. XRD was conducted at 2θ values from 5° to 70° to test the crystalline phases of raw materials and UHPC mixtures. Samples used for the XRD test were grounded into powder with the maximum diameter of 63 μm.

4. Experimental results and discussion

This section presents the test results of the compressive strength, flexural strength, and density of the mixtures and discusses the effects

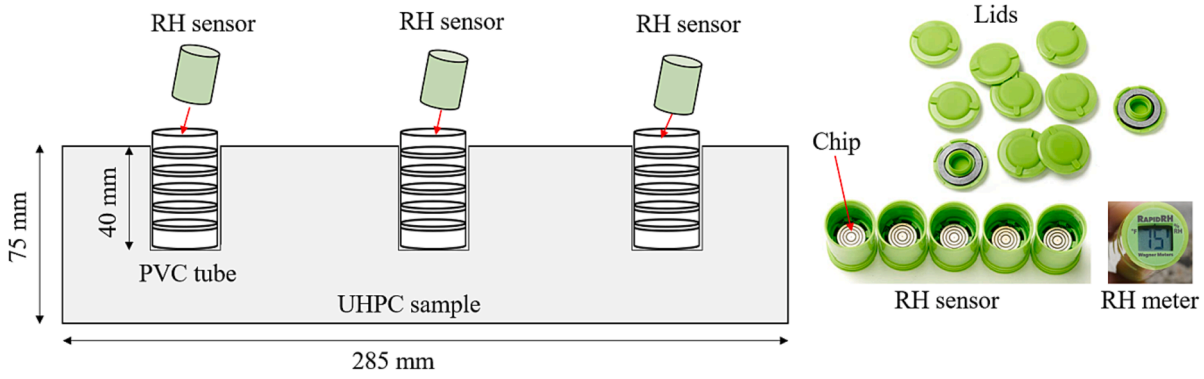

Fig. 3. Experimental setup for relative humidity test.

and mechanisms of glass microsphere, expanded glass, and PE fiber on the test properties. The thermal conductivity results were recorded to evaluate the effects of the lightweight materials on thermal insulation. A comprehensive discussion on strength development of each prepared sample and internal curing effect are made based on the thermal, component, and microstructural results.

4.1. Density and mechanical properties

4.1.1. Compressive strength and density

Fig. 4 shows the test results of the compressive strength up to 91 d. Compare with the control mixture, when glass microsphere was used as 20 % of binder, the 28-d compressive strength decreased from 134.2 MPa to 127.6 MPa, by 5 %. When the steel fibers were fully replaced by the PE fibers, the 28-d compressive strength decreased from 127.6 MPa to 118.3 MPa, by 7 %. When the replacement percentage of the quartz sand by the expanded glass was up to 25 %, the compressive strength increased with the replacement percentage. When the replacement percentage exceeded 25 %, the compressive strength decreased. To note, the mixture with 100 % expanded glass provided 28-d compressive strength higher than 100 MPa, which was sufficient for most structural applications.

Fig. 5 shows the density test results. Compared with the control mixture, when 20 % glass microsphere was used as binder, the density decreased from 2,500 kg/m^3 to 2,286 kg/m^3, by 9.2 %. When the steel fibers were fully replaced by the PE fibers, the density reduced from 2,286 kg/m^3 to 2,178 kg/m^3, by 4.7 %. As the expanded glass content increased from 0 to 100 %, the density reduced from 2,178 kg/m^3 to 1,735 kg/m^3, by 20.3 %.

Fig. 6 compares the compressive strength and density of the UHPC mixtures from this study and the previous lightweight concrete mixtures [5,10,14,41–46]. In general, the compressive strength decreased with the decrease in density. In this study, with extremely low cement content (40 %), the density of the developed UHPC mixtures was as low as 1,750 kg/m^3, which was 30 %-34 % lower than the density of conventional UHPC (2,500–2,650 kg/m^3), while the 28-d compressive strength was retained at 100–127 MPa. Further discussions on the compressive strength are available in Section 4.5.

4.1.2. Flexural strength

Fig. 7(a) shows the load versus the mid-span deflection of specimens at 28 d. Fig. 7(b) plots the flexural strength versus the ultimate deflection. Comparison between the control mixture with mixture GM20 shows that replacing 20 % slag by glass microsphere decreased the flexural strength from 23.9 MPa to 22.0 MPa (by 8 %), while increasing the ultimate deflection from 3.0 mm to 4.6 mm (by 53 %). The comparison of the control mixture with mixture L0 shows that replacing the

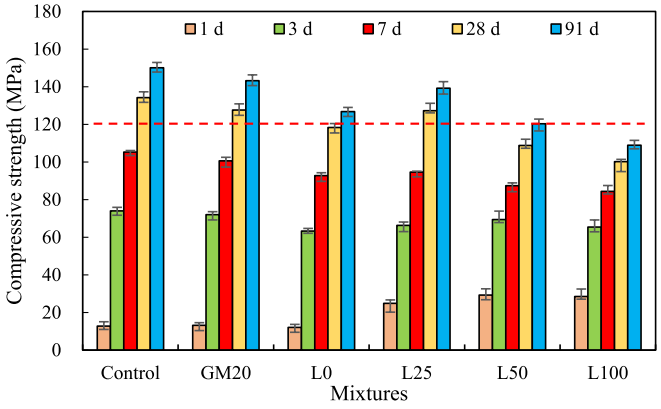

Fig. 4. Test results of compressive strength for prepared UHPC at different ages up to 91 d.

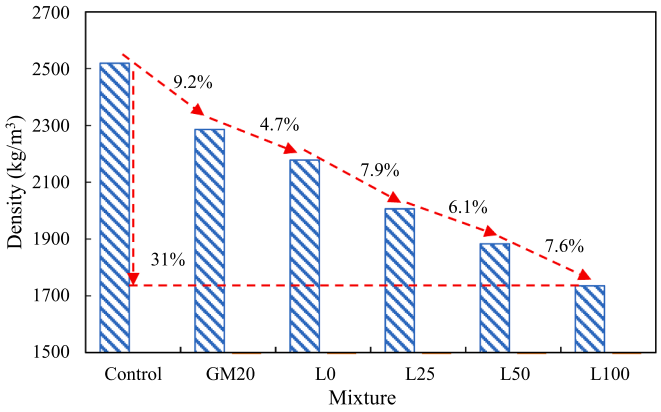

Fig. 5. Test results of the hardened density of UHPC mixtures after the curing for 28 d.

steel fibers with the PE fibers decreased the flexural strength from 22.0 MPa to 18.2 MPa (by 17.3 %), while increasing the ultimate deflection from 4.6 mm to 11.9 mm (by 157 %), indicating that the PE fibers improved the ductility. The comparison of mixtures L0 and L25 shows that using the expanded glass as 25 % aggregate increased the flexural strength from 18.2 MPa to 21.3 MPa, while increasing the ultimate deflection from 11.9 mm to 13.4 mm. As the expanded glass content increased from 25 % to 100 %, the flexural strength decreased from 21.3 MPa to 13.2 MPa, while the ultimate deflection increased from 13.4 mm to 27.5 mm.

The crack patterns of the control mixture and mixture L100 are shown in Fig. 8(a) and (b), respectively. The mixture with steel fibers showed a single major crack (up to 500 μm) when the specimen failed, accompanied by a relatively small deflection (Fig. 7). In Fig. 8(b), the mixture with PE fibers showed dense microcracks, accompanied by higher deflection and toughness. When the specimen failed with localized cracks, crack widths were in the range of 21 μm to 180 μm, and most cracks were in the range of 61 μm to 100 μm. The generation of many fine cracks is attributed to the preferred interfacial properties between the PE fibers and the matrix [47], and reducing the crack width is beneficial for the durability, as elaborated in reference [48]. The permeability of cracked matrix with fine microcracks is comparable with uncrack matrix. Besides, the fine crack width promotes self-healing of the cementitious matrix because there is a higher chance for hydration products to fill fine microcracks.

4.2. Relative humidity and autogenous shrinkage

Fig. 9(a) shows the results of internal relative humidity (IRH). During the first 24 h, the IRH of mixture L100 decreased by 2 %, while the IRH of mixture L0 decreased by 18 %. Up to 168 h, the IRH of mixture L0 was reduced by 29 %, while the IRH of mixture L100 was reduced by only 15 %. The water stored in the pores of expanded glass was released gradually in the internal curing process, thus sustaining a high IRH level.

Fig. 9(b) shows the autogenous shrinkage results. When the expanded glass content increased from 0 to 100 %, the shrinkage was reduced from 809 μm/m to 507 μm/m, by 47 %. The reduction of shrinkage was attributed to the moisture released from the expanded glass, thus mitigating the self-desiccation effect in the UHPC matrix [5]. The relationship between the IRH and the autogenous shrinkage is plotted in Fig. 9(c). The results confirm that the reduction of IRH is the major driver of the autogenous shrinkage.

4.3. Thermal conductivity

Fig. 10(a) plots the results of the thermal conductivity. The use of glass microsphere as 20 % binder reduced the thermal conductivity. The

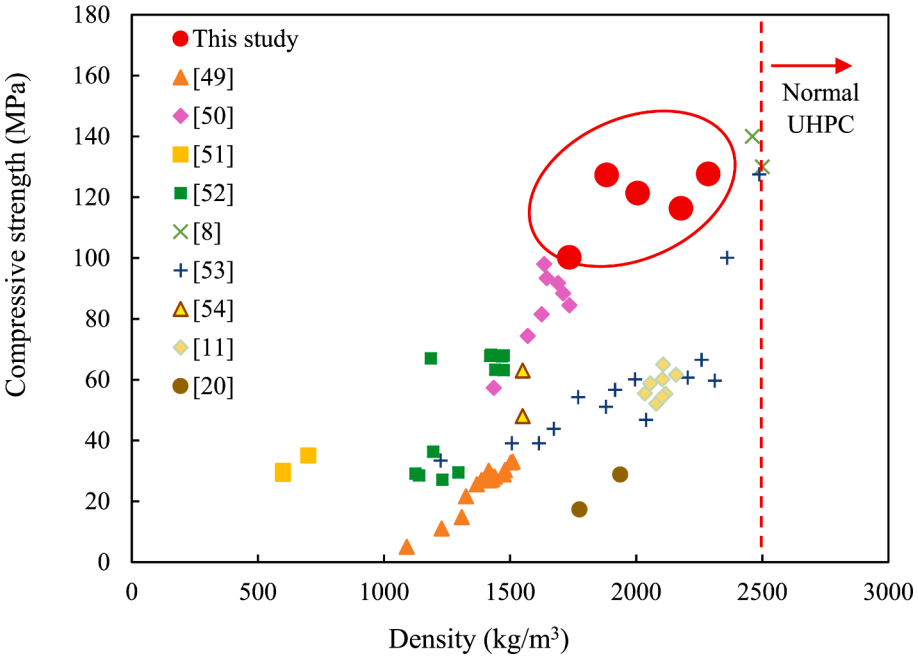

Fig. 6. Statistics of the compressive strength versus the density of the lightweight mixtures.

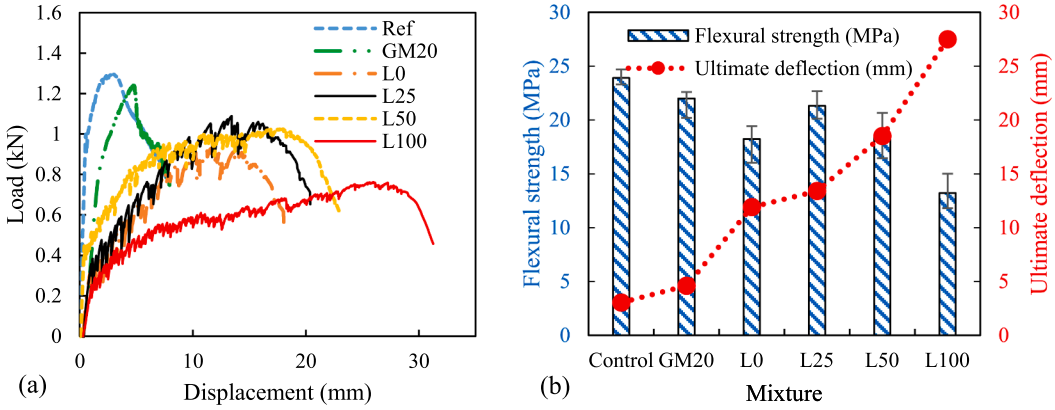

Fig. 7. Test results of: (a) load–deflection curve, and (b) flexural behavior after 28 d of curing.

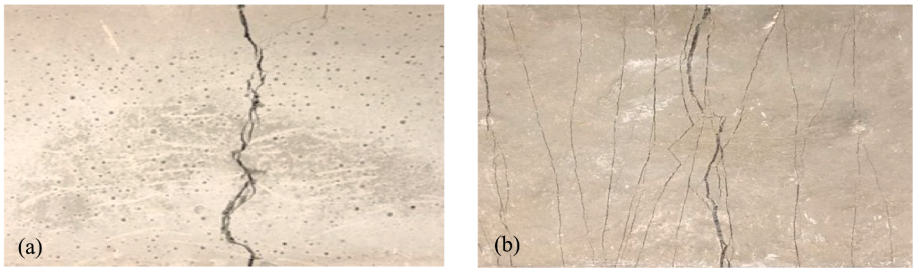

Fig. 8. Comparison of the crack patterns of: (a) the control mixture, and (b) mixture L100.

thermal conductivity of mixture L0 with 20 % glass microsphere was 1.3 W/mK, considerably lower than that of conventional UHPC (2.0 W/mK [49]). With the increase of the expanded glass content from 0 to 100 %, the thermal conductivity decreased from 1.3 W/mK to 0.65 W/mK. Fig. 10(b) shows the correlation between thermal conductivity and density, with a coefficient of determination (R^2) of 0.99. The heat transfer inside UHPC mixtures depends on the collision of phonons. The thermal conductivity is correlated to the mean free path of phonon, which represents the average distance between successive collisions [37]. The increase of defects such as crystal defects, voids, and impurities reduce the mean free path of phonon, thus decreasing the thermal conductivity [50]. The use of porous expanded glass and hollow glass microsphere in preparing UHPC mixtures largely reduced thermal conductivity, making these mixtures promising for desired thermal insulation performance in structural applications. For example, using thermal insulating UHPC in buildings is promising to improve energy

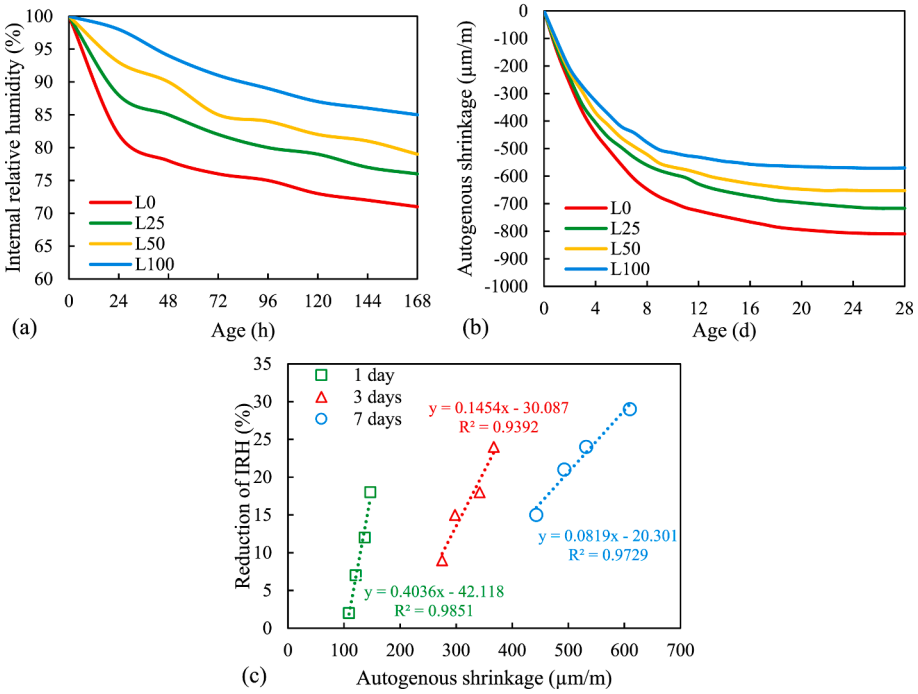

Fig. 9. Test results of IRH and autogenous shrinkage of the tested UHPC mixtures: (a) the IRH up to 7 d, (b) the autogenous shrinkage up to 28 d, and (c) the correlation between the IRH and the autogenous shrinkage at 1 d, 3 d, and 7 d.

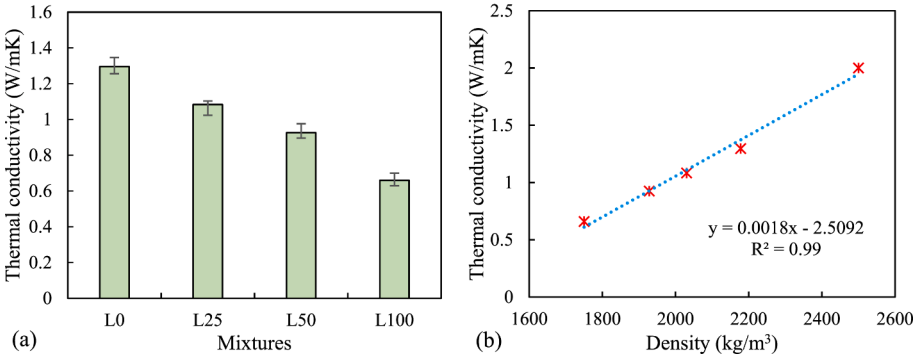

Fig. 10. Thermal insulation analysis for UHPC samples: (a) thermal conductivity, and (b) correlation between thermal conductivity and density.

efficiency.

4.4. Alkali-silica reactivity

Fig. 11 shows the results of the accelerated ASR tests for mixtures L0, L50, and L100. The results of mixtures L0, L50, and L100 were −0.20 %, −0.14 %, and −0.09 %, respectively, at 14 d. Mixtures L0, L50, and L100 showed shrinkage rather than expansion when they were exposed to alkaline solution and high temperature. Such results are attributed to four main reasons: (1) ASR reaction involves the alkalis, such as sodium and potassium ions, reacting with amorphous silica to produce gels. In the ASR tests, the elevated temperature promoted the pozzolanic reaction, which competed with the ASR reaction by consuming amorphous silica and thus reducing the production of ASR gel for expansion. (2) The average particle sizes of glass microsphere and expanded glass were 15 μm and 150 μm, respectively. With such small particle sizes, the pozzolanic reaction was highly promoted. The pozzolanic reaction produced more C—S—H gel and consumed more amorphous silica. (3) The C—S—H gel generated a shell that covered the surfaces of the glass microsphere and the expanded glass, which hindered the dissolution of amorphous silica and the penetration of deleterious cations such as sodium and potassium ions, further suppressing the ASR reaction. (4) The shrinkage of the UHPC mixtures was significantly greater than the ASR expansion, which was attributed to the low water-to-binder ratio of the UHPC mixtures.

4.5. Discussions on underlying mechanisms

Based on the results shown in Section 4, a comprehensive discussion is presented to identify the mechanism of lightweight material on mechanical properties of UHPC. Among the investigated UHPC mixtures, the use of glass microsphere decreased the mechanical properties. As the expanded glass content was increased from 0 to 50 %, the L25 mixture achieved the highest 28-d compressive strength and flexural strength. The increase (L0 to L25) and decrease (L25 to L100) of the compressive strength and flexural strength are dependent on competing mechanisms, as discussed in this section.

4.5.1. Pozzolanic reactivity

The crystallinity of expanded glass aggregate and hollow glass microsphere was identified by XRD analysis, as shown in Fig. 12. Both expanded glass aggregate and hollow glass microsphere were

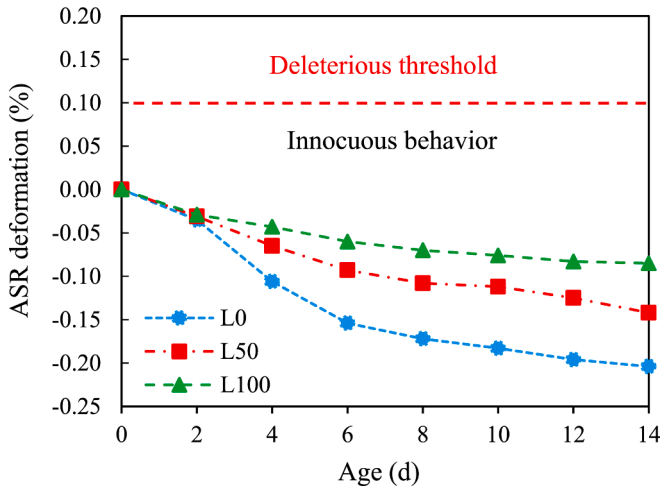

Fig. 11. Test results of the ASR deformations for UHPC mixtures L0, L50, and L100. UHPC is regarded as no ASR expansion when length change of the prism <0.10%.

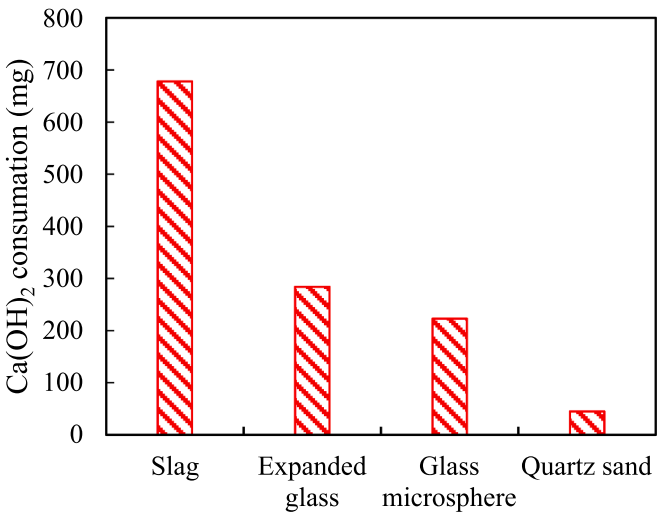

Fig. 13. Results of the pozzolanic reactivity of the raw materials used in the mixtures.

amorphous, indicating that they were chemically reactive. In a high pH condition, the chemical bond of expanded glass aggregate and hollow glass microsphere were broken, which can combine with water and cations, to generate C—S—H gels or ASR gels.

The pozzolanic reactivity of the slag, expanded glass, glass microsphere, and quartz sand are shown in Fig. 13. The CH consumption results of the slag, expanded glass, and glass microsphere were 678 mg, 284 mg, and 223 mg, respectively, indicating that the slag had higher pozzolanic reactivity than the other three types of material.

The test results of the pozzolanic reactivity explained the underlying mechanisms of the reduction of the mechanical strength of the UHPC mixtures. For example, when the slag of the control mixture was replaced by the glass microsphere, the compressive strength of mixture GM20 was lower than that of the control mixture.

4.5.2. *Internal curing effect*

An interesting observation was that the compressive strength and the flexural strength of the UHPC mixtures increased when up to 25 % presaturated expanded glass was used to replace quartz sand, but the compressive strength and the flexural strength decreased when the replacement ratio was higher than 25 %. Competitive effects responsible for this phenomenon are discussed as follows.

The UHPC mixtures has unreacted cement particles and cementitious materials such as slag and glass particles because of the low water-to-binder ratio. The degree of hydration is limited due to the lack of water. With the introduction of internal curing agents, moisture is released due to the osmotic pressure in the hardening process when the water content continuously decreases. In this study, the expanded glass aggregate served as the internal curing that provided internal curing water, increasing the degree of hydration and densifying the microstructures by producing more C—S—H gel. The C—S—H gel filled the pore around the interfacial transition zone (ITZ) while generating a hard shell for expanded glass. With a dense ITZ and hard shell, the brittleness of expanded glass aggregate was mitigated. Therefore, the UHPC matrix was able to withstand higher external loads, as shown in Fig. 14.

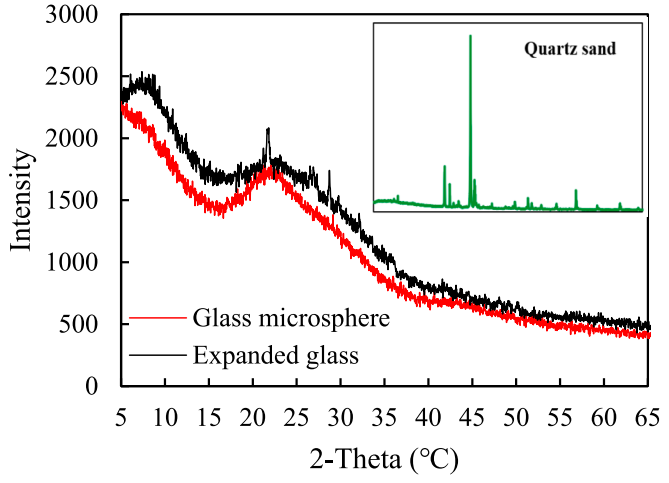

Fig. 12. Results of the crystallinity analysis of the glass microsphere and expanded glass.

When the replacement percentage of expanded glass was high (>25 %), the expanded glass introduced too much porosity, thus reducing the mechanical strengths. As reported by manufacturer, the expanded glass is crushed at 3 MPa load due to the porous structure. In short, the internal curing effect dominates when the replacement percentage is low, and the porosity effect dominates when the replacement percentage is higher than 25 %.

Heat of hydration

The heat of hydration and the cumulative heat of the UHPC mixtures are shown in Fig. 15(a) and (b), respectively. The results show that the increase of the expanded glass content accelerated the hydration reactions by highly shortening the dormant period. This is mainly attributed to the reduction of the HRWR demand in the UHPC mixtures with consistent workability, as shown in Table 4. As the expanded glass content increased from 0 to 100 %, the HRWA dosage decreased from 3.01 % to 1.02 %. Since HRWA retards the hydration of cementitious materials, the reduction of HRWR promoted the hydration, increasing the 1-d and 3-d compressive strength. In addition, the internal curing water of expanded glass facilitates the hydration process.

Thermal analysis

Fig. 16(a) shows the results of TGA. The mass loss increased with the temperature. There were three important points in each curve: The evaporation of free water at 100 °C; the dihydroxylation of CH at 450 °C; and the decomposition of $CaCO_3$ at 680 °C. The mass loss increased with the content of expanded glass aggregate. Fig. 16(b) shows the quantification of CH and bound water of the mixtures. Both the CH and bound water contents increased with the expanded glass content. When the expanded glass content increased from 0 to 100 %, the CH and bound water contents increased by 21.4 % and 31.2 %, respectively. The use of expanded glass aggregate promoted the hydration process due to internal curing.

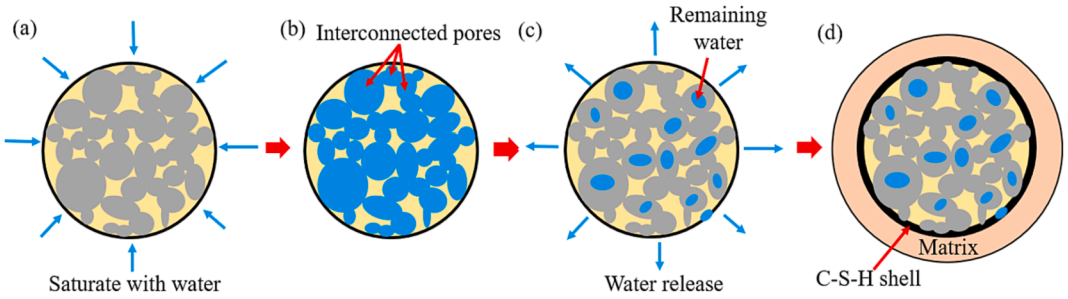

Fig. 14. Internal curing effect of the expanded glass: (a) pre-saturation of the expanded glass (particles soaked in water for 24 h); (b) internal pores occupied by water; (c) release of internal curing water in the hardening process; and (d) promotion of the hydration of the unreacted cementitious materials to produce C—S—H gel.

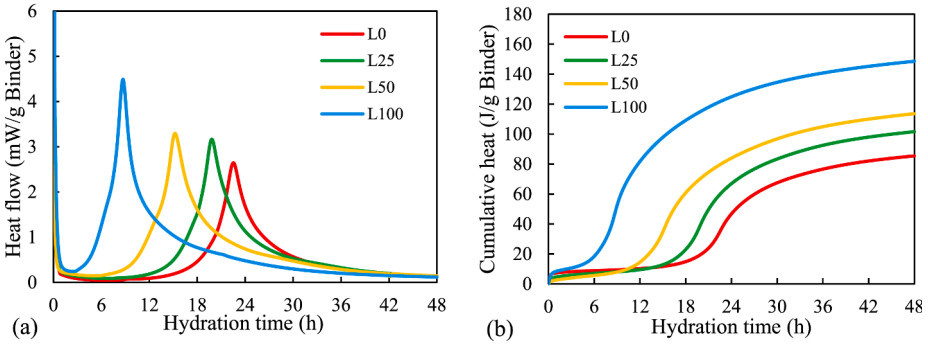

Fig. 15. Isothermal results of UHPC samples: (a) hydration heat and (b) cumulative heat.

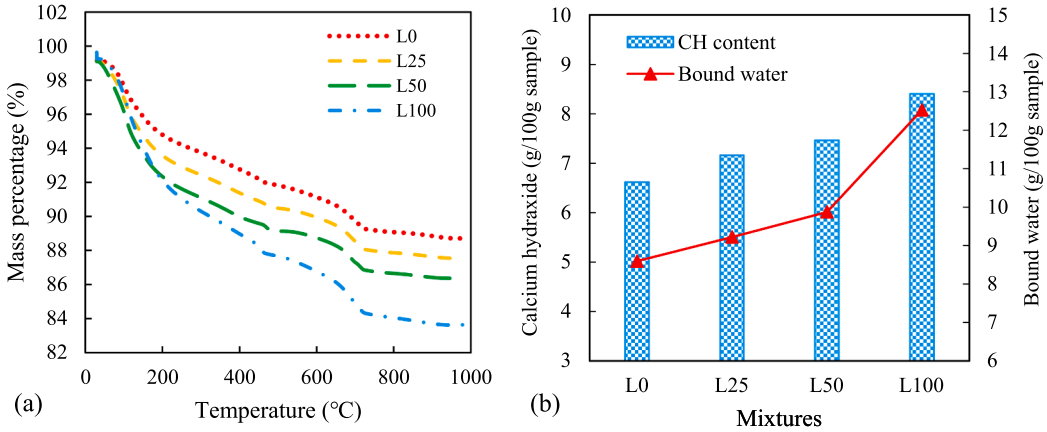

Fig. 16. TGA test results of: (a) mass loss percentage versus temperature and (b) quantification of the CH and bound water contents.

Component analysis

Similar results were found in XRD analysis, as shown in Fig. 17. The main components of prepared samples were quartz, ettringite, CH, and unreacted clinker (C_2S/C_3S). The 2-theta peaks representing CH content were at 18.1°, 34.2°, and 42.8°. The 2-theta peak representing the CH content of mixture L100 was higher than that of mixture L0, indicating a higher degree of hydration. The internal curing facilitated the hydraulic reaction to produce more CH. The 2-theta peak reflecting unreacted clinker included 29.5° and 32.7°. Similarly, increasing the expanded glass content resulted in less unreacted clinker in the samples, indicating a higher degree of hydraulic reaction in the sample due to internal curing.

Pore structure

Fig. 18(a) shows the test results of the pore size distribution. The main pore size was concentrated at 1 nm to 50 nm, indicating dense microstructures of the UHPC samples. Fig. 18(b) plots the total intrusion volume of mercury versus the pore diameter. The discussion of porosity is divided into two aspects: (1) Intuitively, the use of expanded glass increases the porosity, because the expanded glass is porous. However, when up to 25 % expanded glass was used in UHPC, the total pore volume decreased from 0.39 cc/g to 0.37 cc/g. Specifically, the volume of gel pore (<100 nm) increased from 0.33 cc/g to 0.34 cc/g, when the expanded glass content increased from 0 to 25 %. Due to the internal curing effect, the hydraulic reaction was promoted, increasing the volume of gel pores and decreasing the volume of large pores (>100 nm). The porosity of expanded glass was the main source of the large pores. The hydration products developed by the pozzolanic reaction and the cement hydration produce shells to partially seal the surfaces of the expanded glass and prevent the intrusion of mercury. (2) When the usage of expanded glass was higher than 25 %, the hydraulic reaction was promoted by the internal curing effect. As expanded glass content increased from 25 % to 100 %, the volume of the gel pores increased

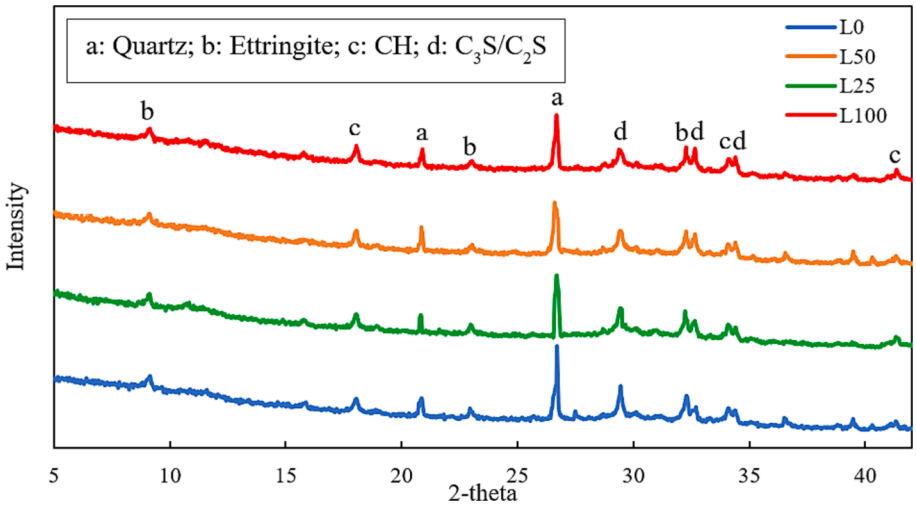

Fig. 17. Measurement results of the XRD patterns of the investigated mixtures at 28 d.

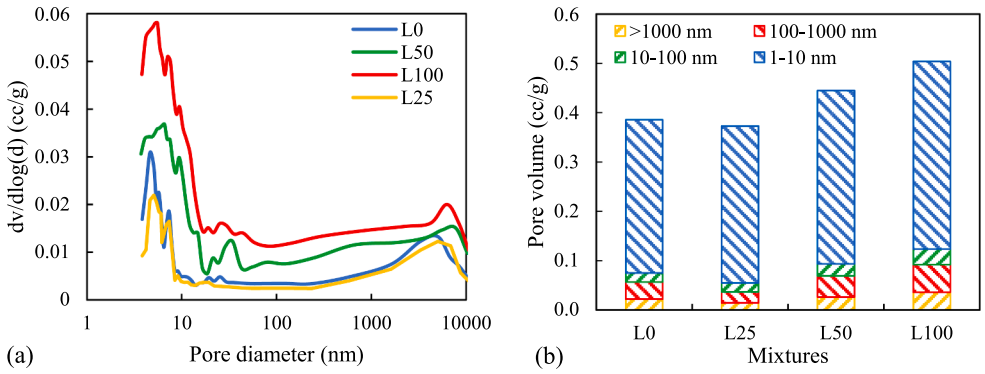

Fig. 18. MIP test results: (a) pore size distribution, and (b) pore volume versus pore size.

from 0.34 cc/g to 0.41 cc/g. However, the volume of large pores increased from 0.04 cc/g to 0.09 cc/g. Not all the expanded glass particles were well-sealed by the hydration products, therefore introducing more large pores. Overall, as the expanded glass content increased from 25 % to 100 %, the total pore volume increased from 0.36 cc/g to 0.50 cc/g. The increased porosity reduced the compressive strength and the flexural strength.

5. Economy and environmental impacts

Annually, about 60 % of waste glass is landfilled, which is not economical and causes pollution to soil and groundwater [33]. Especially, compared with many types of municipal solid waste such as wood and paper, glass is chemically stable and nonbiodegradable over a long time [33]. An alternative method to utilize waste glass is to produce multifunctional materials such as the glass microsphere and expanded glass, which features lightweight and low thermal conductivity. It deserves to conduct a life cycle analysis when the glass microsphere and expanded glass are used in cementitious composites. In addition, when PE fibers are used to replace steel fibers, the economic impact should be considered.

The unit cost, energy consumption, and carbon footprint of the raw materials are listed in Table 5 [34,51–54]. The process of manufacturing expanded glass is similar to that of glass, which includes several steps: (1) treatment of the waste glass, including crushing, drying, and sieving; (2) expansion: adding the expansion agents at 900–1,300 ℃; and (3) cooling [20]. The energy consumption and the CO_2 emission for producing 1 kg expanded glass are assumed as 1.14 MJ and 0.6 kg, respectively [53]. Table 6 shows the mixture design of lightweight UHPC used for cost and environmental analysis.

Table 5
Inventory of cost, energy consumption, and CO_2 emission.

Ingredients	Weight (kg)	Unit price ($)	CO_2 emission (kg)	Energy consumption (MJ)
Cement	1	0.11	0.83	4.73
Slag	1	0.10	0.02	0.08
Silica fume	1	0.40	0.03	0.06
Glass microsphere	1	5.92	0.30	0.18
Expanded glass	1	1.42	0.60	1.14
Glass powder	1	0.10	0.60	1.14
Quartz sand	1	0.03	0.10	0.11
HRWR	1	3.60	0.72	18.30
Water	1	0.04	0.01	0.00
Steel fiber	1	4.76	1.49	20.56
PE fiber	1	16.20	4.08	69.40

5.1. Economic analysis

With the inventory data in Table 5, the unit cost of 1 m^3 UHPC is calculated using Eq. (2) [55]:

$$M = \sum_{i=1}^{n} m_i r_i \quad (2)$$

where M is the unit cost of manufacturing 1 m^3 UHPC mixture; m_i is the

Table 6
UHPC mixture design.

Ingredients	UHP-LCC [6]	Control	GM20	L0	L25	L100
Cement	762	565.1	565.1	565.1	565.1	565.1
Slag	0	780.4	520.3	520.3	520.3	520.3
Silica fume	229	0	0	0	0	0
Glass microsphere	102	0	41.3	41.3	41.3	41.3
Expanded glass	0	0	0	0	56.1	224.3
Glass powder	229	0	0	0	0	0
Quartz sand	0	780.4	780.4	780.4	557.1	0
HRWR	60	40.5	34	34	28.4	11.5
Water	135	225.1	227.9	227.9	232.6	243.6
Steel fiber	130	117	117	0	0	0
PE fiber	0	0	0	14.6	14.6	14.6

unit cost of the i^{th} ingredient *(I = 1, 2, 3, …, n)*; and r_i is the mass of the i^{th} ingredient.

The strength-normalized cost ($/m^3/MPa) was used to evaluate the cost-effectiveness of UHPC mixtures through combination of the 28-d compressive strength and unit cost. Fig. 19(a) plots the cost and the strength-normalized cost. Compared with mixture UHP-LCC in reference [6], the UHPC mixtures proposed in this study are more cost-effective. The use of glass microsphere in mixture GB50 decreased the unit cost from 1,733 $/m^3 to 1,112 $/m^3 (by 36 %), and decreased the strength-normalized cost from 14.2 $/m^3/MPa to 8.7 $/m^3/MPa (by 39 %). When the steel fibers were replaced by the PE fibers in mixture L0, the unit cost further decreased from 1,112 $/m^3 to 791 $/m^3 (by 29 %), and the strength-normalized cost deceased from 8.7 $/m^3/MPa to 6.7 $/m^3/MPa (by 23 %). As the expanded glass content increased from 0 to 25 %, the unit cost and the strength-normalized cost were retained; however, as the expanded glass content increased from 25 % to 100 %, the unit cost and the strength-normalized cost increased. Mixture L0 achieved the lowest unit cost (791 $/m^3), which is 10 % lower than that of the control mixture. Meanwhile, mixture L0 has much lower density than the control mixture (Fig. 19(b)). The size of each bubble represents the unit cost of a mixture. Among these mixtures, mixture L25 achieved high compressive strength, low density, and low cost.

5.2. Carbon emission

The carbon emission of each mixture was evaluated using Equation (3) [55]:

$$C = \sum_{i=1}^{n} c_i r_i \tag{3}$$

where C is the CO_2 emission of manufacturing 1 m^3 UHPC mixture; c_i is the CO_2 emission of manufacturing the i^{th} ingredient ($i = 1, 2, 3, \ldots, n$); and r_i is the mass of the i^{th} ingredient.

Fig. 20(a) shows the carbon emission and the strength-normalized carbon emission. Compared with mixture UHP-LCC [6], the UHPC mixtures in this study had lower carbon emission. The use of glass microsphere in mixture GB50 decreased the unit carbon emission from 1,046 kg/m^3 to 771 kg/m^3 (by 26 %), and decreased the strength-normalized emission from 8.7 kg/m^3/MPa to 6.0 kg/m^3/MPa (by 31 %). When the steel fibers were replaced by PE fibers in mixture L0, the unit emission further decreased from 771 kg/m^3 to 656 kg/m^3 (by 15 %), and the strength-normalized emission deceased from 8.7 kg/m^3/MPa to 5.5 kg/m^3/MPa (by 37 %). As the expanded glass content increased from 0 to 100 %, the unit carbon emission slightly decreased, and the strength-normalized emission first increased and then decreased. Mixture L0 achieved the lowest strength-normalized carbon emission (5.5 kg/m^3/MPa), which is slightly lower than that of the control mixture. Meanwhile, mixture L0 has much lower density than the control mixture (Fig. 20(b)). The size of each bubble represents the unit carbon emission of a mixture. Among these mixtures, mixture L25 achieved high compressive strength, low density, and low carbon emission.

5.3. Energy efficiency

The energy consumption of each mixture was evaluated by Eq. (4) [55]:

$$E = \sum_{i=1}^{n} e_i r_i \tag{4}$$

where E is the equivalent energy consumption of manufacturing 1 m^3 UHPC mixture; e_i is the energy consumption used to manufacture the i^{th} ingredient *(I = 1, 2, 3, …, n)*; and r_i is the mass of the i^{th} ingredient.

The energy efficiency of the mixtures was assessed by the strength-normalized energy consumption (unit in MJ/m^3/MPa). Fig. 21(a) plots the energy consumption and strength-normalized energy consumption. Compared with mixture UHP-LCC [6], the mixtures in this study had lower carbon footprint.

The use of glass microsphere in mixture GB50 decreased the unit energy consumption from 7,432 MJ/m^3 to 5,828 MJ/m^3 (by 22 %), and decreased the strength-normalized energy consumption from 61 MJ/m^3/MPa to 45 MJ/m^3/MPa (by 26 %). When the steel fibers were replaced by PE fibers in mixture L0, the unit energy consumption further decreased from 5,828 MJ/m^3 to 4,435 MJ/m^3 (by 24 %), and the strength-normalized energy consumption deceased from 45 MJ/m^3/MPa to 37 MJ/m^3/MPa (by 18 %). As the expanded glass content increased from 0 to 100 %, the unit energy consumption slightly decreased, and the strength-normalized energy consumption first

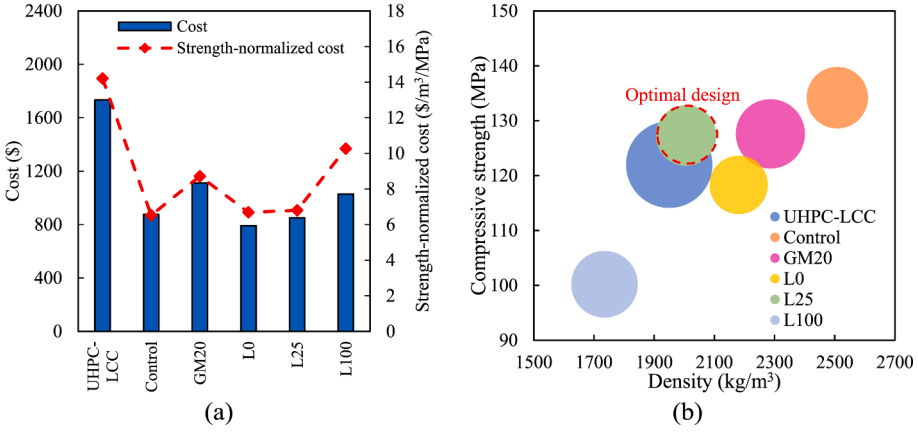

Fig. 19. Life-cycle analysis results of (a) the unit cost and the strength-normalized cost, and (b) the compressive strength, the density, and the unit cost.

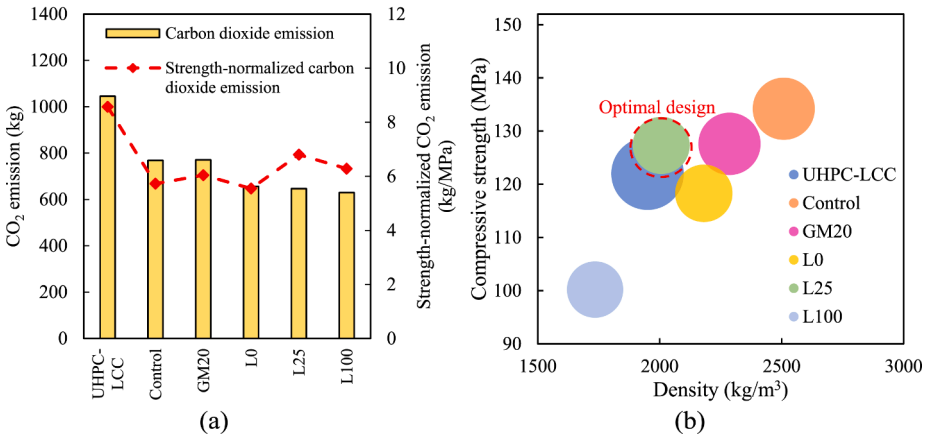

Fig. 20. Life-cycle analysis results of: (a) the CO_2 emission and the strength-normalized CO_2 emission, and (b) the compressive strength, the density, and the CO_2 emission.

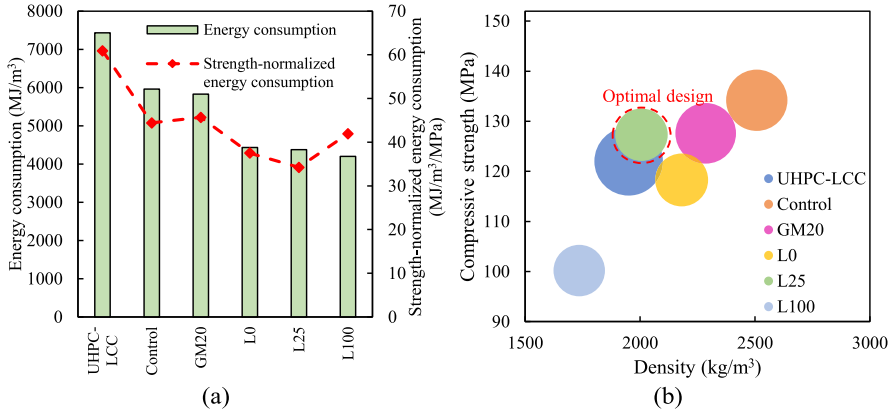

Fig. 21. Life-cycle analysis results of: (a) the energy consumption and the strength-normalized energy consumption, and (b) the compressive strength, the density, and the energy consumption.

decreased and then increased. Mixture L0 achieved the lowest strength-normalized energy consumption (37 MJ/m^3/MPa), which is 18 % lower than that of the control mixture (45 MJ/m^3/MPa). Meanwhile, mixture L0 has lower density than the control mixture (Fig. 21(b)). The size of each bubble represents the unit energy consumption of a mixture. Among these mixtures, mixture L25 achieved high compressive strength, low density, and low energy consumption.

5.4. Comparison between steel and PE fiber

Fig. 22 plots the radar chart of the cost, the energy consumption, the carbon emission, the compressive strength, and the density of mixtures GM20 and L0. Mixtures GM20 and L0 contain 1.5 % of steel fiber and PE fiber, respectively. All other raw ingredients for mixtures GM20 and L0 are consistent. The radar chart area of mixture L0 was significantly smaller than the area of mixture GM20, meaning that mixture L0 was more cost-effective and sustainable than mixture GM20.

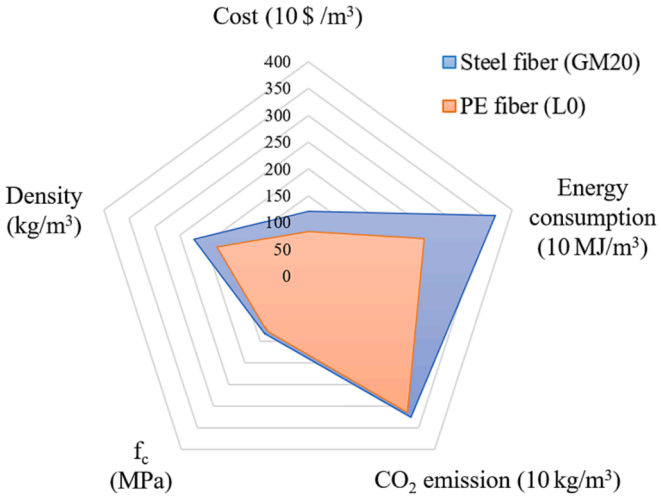

Fig. 22. Comparison of the radar charts of UHPC mixtures GM20 and L0 in this research.

6. Conclusion

This paper presents a new approach to develop lightweight UHPC with low density, low cost, low carbon footprint, low energy consumption, low thermal conductivity, high mechanical strengths, and high ductility, namely sustainable and lightweight UHPC, by using hollow glass microsphere, expanded glass aggregate, and PE fibers. The sustainability is improved through reducing the density, cost, carbon footprint, embodied energy, and thermal conductivity and increasing the ductility while retaining the mechanical strengths. Comprehensive experiments and life cycle assessment is performed to investigate the benefits of adopted raw materials. Based on the above investigations, the following conclusions are drawn:

(1) By using 20 % glass microsphere as binder, 25 % expanded glass as aggregate, and 1.5 % PE fiber as reinforcement, the UHPC mixture achieved high compressive strength (127 MPa), high flexural strength (21 MPa), and low density (2,006 kg/m^3). The life-cycle cost, carbon emission, and embodied energy were estimated to be 850 \$/m^3, 647 kg/m^3, and 4,374 MJ/m^3, respectively.
(2) Expanded glass is able to serve as lightweight aggregate to reduce the density, mitigate the autogenous shrinkage and enhance the mechanical strengths of UHPC through internal curing. The use of expanded glass retained the IRH at a high level during the hardening of the matrix by gradually releasing internal curing moisture. The use of expanded glass is able to reduce the thermal conductivity and improve the thermal insulation performance of UHPC. With 100 % expanded glass, the thermal conductivity reduced by 49 %.
(3) The use of glass microsphere and expanded glass did not cause detrimental ASR problem to the lightweight UHPC mixtures. When 20 % glass microsphere and 100 % expanded glass were respectively used as the binder and the fine aggregate, ASR expansion did not occur; and, instead, shrinkage was measured as 0.09 % at 14 d. The ASR effect was hindered by the dense microstructures of the developed UHPC mixtures, the fine sizes of glass particles, and the autogenous shrinkage of UHPC mixtures due to the low water-to-binder ratios.
(4) Replacing the steel fibers by the PE fibers largely improved the ductility of UHPC mixtures by promoting the generation of dense microcracks in the matrix while reducing the density, cost, carbon footprint, and embodied energy of UHPC. The dense microcracks benefit long-term durability due to the reduced crack widths.

CRediT authorship contribution statement

Pengwei Guo: Data curation, Formal analysis, Visualization, Writing – original draft. **Weina Meng:** Conceptualization, Funding acquisition, Resources, Methodology, Supervision, Writing – review & editing. **Jiang Du:** Formal analysis, Writing – review & editing. **Lily Stevenson:** Data curation, Writing – review & editing. **Baoguo Han:** Formal analysis, Writing – review & editing. **Yi Bao:** Conceptualization, Project administration, Supervision, Writing – review & editing.

Declaration of Competing Interest

The authors declare that they have no known competing financial interests or personal relationships that could have appeared to influence the work reported in this paper.

Data availability

Data will be made available on request.

Acknowledgement

This research was funded by United States National Science Foundation (award number: CMMI-2046407) and New Jersey Department of Transportation through the Bridge Resource Program (contract number: 21-50862). The authors thank Mr. Bill Kulish (President of Steelike lnc) for donating steel fibers and Minifibers for donating polyethylene fiber.

References

[1] K.H. Khayat, W. Meng, K. Vallurupalli, L. Teng, Rheological properties of ultra-high-performance concrete—An overview, Cem. Concr. Res. 124 (2019), 105828.
[2] J. Du, W. Meng, K.H. Khayat, Y. Bao, P. Guo, Z. Lyu, A. Abu-obeidah, H. Nassif, H. Wang, New development of ultra-high-performance concrete (UHPC), Compos. B Eng. 224 (2021), 109220.
[3] W. Meng, K.H. Khayat, Improving flexural performance of ultra-high-performance concrete by rheology control of suspending mortar, Compos. B Eng. 117 (2017) 26–34.
[4] J. Piérard, B. Dooms, N. Cauberg, Durability evaluation of different types of UHPC. Proceedings of the RILEM-fib-AFGC International Symposium on Ultra-High Performance Fiber-Reinforced Concrete, 2013: p. 275-284.
[5] W. Meng, K. Khayat, Effects of saturated lightweight sand content on key characteristics of ultra-high-performance concrete, Cem. Concr. Res. 101 (2017) 46–54.
[6] J.-X. Lu, P. Shen, H. Zheng, H.A. Ali, C.S. Poon, Development and characteristics of ultra high-performance lightweight cementitious composites (UHP-LCCs), Cem. Concr. Res. 145 (2021), 106462.
[7] IN EN 13055 Lightweight aggregates - Part 1: Lightweight aggregates for concrete, mortar and grout.
[8] F. Aslani, L. Wang, M. Zheng, The effect of carbon nanofibers on fresh and mechanical properties of lightweight engineered cementitious composite using hollow glass microspheres, J. Compos. Mater. 53 (17) (2019) 2447–2464.
[9] L. Wang, F. Aslani, I. Hajirasouliha, E. Roquino, Ultra-lightweight engineered cementitious composite using waste recycled hollow glass microspheres, J. Clean. Prod. 249 (2020), 119331.
[10] A.N. Al-Gemeel, Y. Zhuge, O. Youssf, Use of hollow glass microspheres and hybrid fibres to improve the mechanical properties of engineered cementitious composite, Constr. Build. Mater. 171 (2018) 858–870.
[11] Z. Zhang, A. Yuvaraj, J. Di, S. Qian, Matrix design of light weight, high strength, high ductility ECC, Constr. Build. Mater. 210 (2019) 188–197.
[12] A. Hanif, Z. Lu, Z. Li, Utilization of fly ash cenosphere as lightweight filler in cement-based composites–A review, Constr. Build. Mater. 144 (2017) 373–384.
[13] S. Grzeszczyk, G. Janus, Lightweight reactive powder concrete containing expanded perlite, Materials 14 (12) (2021) 3341.
[14] O. Sengul, S. Azizi, F. Karaosmanoglu, M.A. Tasdemir, Effect of expanded perlite on the mechanical properties and thermal conductivity of lightweight concrete, Energy 43 (2–3) (2011) 671–676.
[15] X. Wang, D. Wu, Q. Geng, D. Hou, M. Wang, L. Li, P. Wang, D. Chen, Z. Sun, Characterization of sustainable ultra-high performance concrete (UHPC) including expanded perlite, Constr. Build. Mater. 303 (2021), 124245.
[16] J.-X. Lu, P. Shen, H.A. Ali, C.S. Poon, Development of high performance lightweight concrete using ultra high performance cementitious composite and different lightweight aggregates, Cem. Concr. Compos. 124 (2021), 104277.
[17] A.M. Rashad, Lightweight expanded clay aggregate as a building material–An overview, Constr. Build. Mater. 170 (2018) 757–775.
[18] P. Sikora, T. Rucinska, D. Stephan, S.-Y. Chung, M. Abd Elrahman, Evaluating the effects of nanosilica on the material properties of lightweight and ultra-lightweight concrete using image-based approaches, Constr. Build. Mater. 264 (2020), 120241.
[19] C. Burbano-Garcia, A. Hurtado, Y.F. Silva, S. Delvasto, G. Araya-Letelier, Utilization of waste engine oil for expanded clay aggregate production and assessment of its influence on lightweight concrete properties, Constr. Build. Mater. 273 (2021), 121677.
[20] S.K. Adhikary, D.K. Ashish, Ž. Rudžionis, Expanded glass as light-weight aggregate in concrete–A review, J. Clean. Prod. 313 (2021), 127848.
[21] K. Chahour, D. Aboutaleb, B. Safi, T. Mazari, M. Zeghad, Granulated foam glass based on mineral wastes used for building materials, Build. Acoust. 24 (4) (2017) 281–294.
[22] M. Kurpińska, E. Haustein, Experimental study of the resistance to influence of aggressive liquids on lightweight concrete, Materials 14 (15) (2021) 4185.
[23] A.M. Rashad, A short manual on natural pumice as a lightweight aggregate, J. Build. Eng. 25 (2019), 100802.
[24] J.-X. Lu, H.A. Ali, Y. Jiang, X. Guan, P. Shen, P. Chen, and C.S. Poon, A novel high-performance lightweight concrete prepared with glass-UHPC and lightweight microspheres: Towards energy conservation in buildings. Compos. Part B: Eng., 2022: p. 110295.
[25] D.P. Bentz, P. Lura, J.W. Roberts, Mixture proportioning for internal curing, Concr. Int. 27 (2) (2005) 35–40.
[26] V.C. Li, High-performance and multifunctional cement-based composite material, Engineering 5 (2) (2019) 250–260.
[27] X. Li, J. Wang, Y. Bao, G. Chen, Cyclic behavior of damaged reinforced concrete columns repaired with high-performance fiber-reinforced cementitious composite, Eng. Struct. 136 (2017) 26–35.
[28] S. Rico, R. Farshidpour, F.M. Tehrani, State-of-the-art report on fiber-reinforced lightweight aggregate concrete masonry, Adv. Civil Eng. 2017 (2017) 1–9.
[29] K. Cuevas, M. Lopez, The effect of expansive agent and cooling rate in the performance of expanded glass lightweight aggregate as an internal curing agent, Constr. Build. Mater. 271 (2021), 121505.
[30] K. Al-Sahlani, M. Taherishargh, E. Kisi, T. Fiedler, Controlled shrinkage of expanded glass particles in metal syntactic foams, Materials 10 (9) (2017) 1073.
[31] Y. Zhang, Y. Hua, X. Zhu, Investigation of the durability of eco-friendly concrete material incorporating artificial lightweight fine aggregate and pozzolanic minerals under dual sulfate attack, J. Clean. Prod. 331 (2022), 130022.
[32] W. Meng, M. Valipour, K.H. Khayat, Optimization and performance of cost-effective ultra-high performance concrete, Mater. Struct. 50 (1) (2017) 1–16.
[33] P. Guo, W. Meng, H. Nassif, H. Gou, Y. Bao, New perspectives on recycling waste glass in manufacturing concrete for sustainable civil infrastructure, Constr. Build. Mater. 257 (2020), 119579.
[34] J. Du, Z. Liu, C. Christodoulatos, M. Conway, Y. Bao, W. Meng, Utilization of off-specification fly ash in preparing ultra-high-performance concrete (UHPC): Mixture design, characterization, and life-cycle assessment, Resour. Conserv. Recycl. 180 (2022), 106136.

[35] M. Gesoglu, E. Güneyisi, G.F. Muhyaddin, D.S. Asaad, Strain hardening ultra-high performance fiber reinforced cementitious composites: Effect of fiber type and concentration, Compos. B Eng. 103 (2016) 74–83.
[36] Testing hardened concrete-Part 5: Flexural strength of test specimens. *BS En*: p. 12390-52009.
[37] X. Li, Y. Bao, L. Wu, Q. Yan, H. Ma, G. Chen, H. Zhang, Thermal and mechanical properties of high-performance fiber-reinforced cementitious composites after exposure to high temperatures, Constr. Build. Mater. 157 (2017) 829–838.
[38] ASTM C1609 Standard Test Method for Flexural Performance of Fiber-Reinforced Concrete.
[39] A.L. Brooks, Y. He, N. Farzadnia, S. Seyfimakrani, H. Zhou, Incorporating PCM-enabled thermal energy storage into 3D printable cementitious composites, Cem. Concr. Compos. 129 (2022), 104492.
[40] M.D. Lepech, V.C. Li, R.E. Robertson, G. Keoleian, Design of green engineered cementitious composites for improved sustainability, ACI Mater. J. 105 (6) (2008) 567.
[41] F. Blanco, P. García, P. Mateos, J. Ayala, Characteristics and properties of lightweight concrete manufactured with cenospheres, Cem. Concr. Res. 30 (11) (2000) 1715–1722.
[42] M.H. Zhang, O.E. Gjvorv, Mechanical properties of high-strength lightweight concrete, ACI Mater. J. 88 (3) (1991) 240–247.
[43] L. Wei, W. Zuo, H. Pan, K. Lyu, W. Zhang, W. She, Rational design of lightweight cementitious composites with reinforced mechanical property and thermal insulation: Particle packing, hot pressing method, and microstructural mechanisms, Compos. B Eng. 226 (2021), 109333.
[44] J.-Y. Wang, K.-S. Chia, J.-Y.-R. Liew, M.-H. Zhang, Flexural performance of fiber-reinforced ultra lightweight cement composites with low fiber content, Cem. Concr. Compos. 43 (2013) 39–47.
[45] H. Zhou, A.L. Brooks, Thermal and mechanical properties of structural lightweight concrete containing lightweight aggregates and fly-ash cenospheres, Constr. Build. Mater. 198 (2019) 512–526.
[46] B. Xi, Y. Zhou, K. Yu, B. Hu, X. Huang, L. Sui, F. Xing, Use of nano-SiO2 to develop a high performance green lightweight engineered cementitious composites containing fly ash cenospheres, J. Clean. Prod. 262 (2020), 121274.
[47] K. Yu, Y. Ding, J. Liu, Y. Bai, Energy dissipation characteristics of all-grade polyethylene fiber-reinforced engineered cementitious composites (PE-ECC), Cem. Concr. Compos. 106 (2020), 103459.
[48] Y.i. Bao, M. Valipour, W. Meng, K.H. Khayat, G. Chen, Distributed fiber optic sensor-enhanced detection and prediction of shrinkage-induced delamination of ultra-high-performance concrete overlay, Smart Mater. Struct. 26 (8) (2017) 085009.
[49] A. Dixit, S. Dai Pang, S.-H. Kang, J. Moon, Lightweight structural cement composites with expanded polystyrene (EPS) for enhanced thermal insulation, Cem. Concr. Compos. 102 (2019) 185–197.
[50] M. Razeghi, Fundamentals of solid state engineering. 2006. Available from: https://link.springer.com/book/10.1007/978-0-387-92168-6.
[51] M. Delogu, L. Zanchi, S. Maltese, A. Bonoli, M. Pierini, Environmental and economic life cycle assessment of a lightweight solution for an automotive component: A comparison between talc-filled and hollow glass microspheres-reinforced polymer composites, J. Clean. Prod. 139 (2016) 548–560.
[52] S. Mahjoubi, R. Barhemat, P. Guo, W. Meng, Y. Bao, Prediction and multi-objective optimization of mechanical, economical, and environmental properties for strain-hardening cementitious composites (SHCC) based on automated machine learning and metaheuristic algorithms, J. Clean. Prod. 329 (2021), 129665.
[53] P. Guo, Y. Bao, W. Meng, Review of using glass in high-performance fiber-reinforced cementitious composites, Cem. Concr. Compos. 120 (2021), 104032.
[54] S.S. Muthu, Assessing the Environmental Impact of Textiles and the Clothing Supply Chain. Available from: https://www.sciencedirect.com/book/9780128197837/assessing-the-environmental-impact-of-textiles-and-the-clothing-supply-chain#book-description.
[55] X. Li, X. Lv, X. Zhou, W. Meng, Y. Bao, Upcycling of waste concrete in eco-friendly strain-hardening cementitious composites: Mixture design, structural performance, and life-cycle assessment, J. Clean. Prod. 330 (2022), 129911.